Journal of Alloys and Compounds 509 (2011) 1677–1682

Contents lists available at ScienceDirect

Journal of Alloys and Compounds

journal homepage: www.elsevier.com/locate/jallcom

Chemically synthesized hydrous RuO_2 thin films for supercapacitor application

U.M. Patil, S.B. Kulkarni, V.S. Jamadade, C.D. Lokhande*

Thin Film Physics Laboratory, Department of Physics, Shivaji University, Kolhapur 416004, Maharashtra, India

ARTICLE INFO

Article history:
Received 23 August 2010
Received in revised form
22 September 2010
Accepted 22 September 2010
Available online 29 September 2010

Keywords:
CBD method
Hydrous RuO_2 thin film
Optical properties
Surface morphology
Supercapacitor

ABSTRACT

The hydrous RuO_2 thin films have been successfully synthesized at low temperature on glass and stainless steel substrates using lucrative chemical bath deposition (CBD) method. Their structural, morphological, optical, electrical and wettability properties were studied by means of X-ray diffraction (XRD), scanning electron microscopy (SEM), Fourier transform infrared (FT-IR), UV–vis–NIR spectrophotometer, two point probe method and water contact angle measurement techniques. The results showed that, the CBD method allows to formation of amorphous, porous, superhydrophilic, semiconducting, hydrous RuO_2 thin films with optical band gap of 2.7 eV. The supercapacitive behavior of hydrous RuO_2 in 0.5 M H_2SO_4 electrolyte examined by cyclic voltammetric (CV) measurements showed maximum specific capacitance of 73 $F g^{-1}$.

1. Introduction

Ruthenium dioxide (RuO_2) has been recognized as an important material for a wide range of electrochemical applications because of unique properties [1]. The RuO_2 in both amorphous and crystalline forms has been widely recognized as a potential electrode material in several fields, such as the chloro-alkali industry, water electrolysis, oxygen reduction, organic synthesis, waste effluents, electronics, electrocatalysis, and supercapacitors [2–6]. Also it has been investigated as a cathode material for H_2 evolution, with the advantage of lower sensitivity to poisoning than the more familiar noble-metal catalysts [2]. RuO_2 (or rather the hydrous surface of crystalline, rutile RuO_2) is a desirable electrocatalyst, due to its low overpotentials for O_2 and Cl_2 evolution [7,8]. Anhydrous RuO_2 is a d-band metallic conductor, with a single-crystal conductivity of 10^4 S cm^{-1}. Hydrous forms of RuO_2 designated as RuOxHy or as $RuO_2 \cdot nH_2O$ are also conductive, in the order of 1 S cm^{-1} [9]. More recent studies demonstrate the importance of hydrous RuO_2 in Pt–Ru direct methanol fuel cell catalysts [10].

Galizzioli et al. [11] first recognized that the current response of thermally prepared anhydrous RuO_2 film was similar to that of an ideal capacitor. In recent years, the use of hydrous RuO_2 as an electrode material was investigated. It was found that powder form of amorphous and hydrous RuO_2 prepared by sol–gel method is a promising for supercapacitor with high power density and energy density [12–14]. RuO_2 can be synthesized by various methods such as thermal decomposition, sol–gel process, electrostatic spray deposition (ESD), electrodeposition, etc. [13–16]. Though the hydrous RuO_2 exhibits excellent pseudocapacitive behavior with large specific capacitance and good reversibility, the low abundance and high cost of the precious metal are major limitations to commercial application [17,18].

Alternatively, one can fabricate the RuO_2 electrode by a method having high yield, i.e. by a method that can deposit material on large area at expense of small quantity of initial ingredients. Accordingly, a simple method with high product yield is worthy of being developed. One such method is chemical bath deposition (CBD) method, has been well developed to fabricate large-area thin films in view of its several advantages: it does not require sophisticated instruments; the starting chemicals are commonly available and cheap; the preparation parameters are easily controlled, etc. [19,20].

To the best of our knowledge there is no report on chemical bath deposition of hydrous RuO_2 thin films for supercapacitor application. The supercapacitive properties of the hydrous RuO_2 films (on stainless steel substrate) were studied and reported.

2. Experimental details

Preparation of RuO_2 thin film by CBD method is based on the heating of an acidic bath of complexed ruthenium (III) chloride containing the substrates immersed vertically in the solution. Acidic bath was prepared by using 0.01 M $RuCl_3 \cdot nH_2O$ as a source of ruthenium and 0.1 M ammonium chloride (NH_4Cl) as a complexing agent. The pH of the resultant solution was 2.0. The glass and stain-

* Corresponding author. Tel.: +91 231 2609225.
E-mail address: l.chandrakant@yahoo.com (C.D. Lokhande).

0925-8388/$ – see front matter © 2010 Elsevier B.V. All rights reserved.
doi:10.1016/j.jallcom.2010.09.133

less steel substrates were immersed in the bath placed at 333 K. When the bath attained the temperature of 333 K, the precipitation (blakish in color) started in the bath. During the precipitation, heterogeneous reaction occurred and deposition of RuO_2 took place on the substrate. Before use the substrates were cleaned with laboline detergent, thoroughly washed with double distilled water (DDW) and boiled in dilute chromic acid. Finally these substrates were sonicated in water bath for 15 min. The films on glass substrate were used for structural, morphological and optical studies and the films on stainless steel substrate were utilized for supercapacitor studies.

Structural identification of RuO_2 films were carried out with X-ray diffractometer (XRD) [Cu target ($\lambda = 1.54056$ Å)]. The FT-IR spectrum of the samples were collected using a 'Perkin-Elmer, FT-IR Spectrum one' unit. The microstructures of films were examined with a scanning electron microscope (SEM) (JEOL-JAPAN 6360). Room temperature optical transmission spectrum of samples was recorded in the wavelength range of 350–650 nm using spectrophotometer-119. A two probe method was used for dark electrical resistivity measurement. Electrochemical analysis of the films was studied by cyclic voltammetry (CV) using a potentiostat (263A EG&G, Princeton Applied Research Potentiostat). The half supercapacitor cell comprises platinum as a counter electrode, saturated calomel (SCE) as reference electrode and a hydrous RuO_2 as working electrode immersed in 0.5 M H_2SO_4 electrolyte.

3. Results and discussion

3.1. Thin film formation and reaction mechanism

In CBD method, film formation starts when the solution is saturated. When the ionic product of anion and cation exceeds the solubility product of metal oxide, precipitation occurs and ions combine on the substrate and in the solution to form nuclei. The film growth can take place via ion-by-ion condensation (homogenous nucleation) of materials or by adsorption of colloidal particles (heterogeneous nucleation) from the solution on the substrate. The formation of solid phase from solution involves two steps as nucleation and particle growth. Nucleation is necessary for a precipitate formation. The concept of nucleation in the solution implies, the clusters of molecules formed undergo rapid decomposition and particles combine to grown up to a certain thickness of the film.

Generally metal ions complexed in such a way that, reaction takes place between slowly released metal ions to form product in thin film. The RuO_2 thin film depositions take place on glass and steel substrates via slow hydrolysis of ruthenium chloride solution. This can be represented as follows:

$$RuCl_3 + 3H_2O \rightarrow Ru(OH)_3{}^+ + 3HCl \quad (1)$$

$$Ru(OH)_3{}^+ + NH_4Cl \leftrightarrow (NH_3)Ru(OH)_3{}^+ + HCl \quad (2)$$

$$(NH_3)Ru(OH)_3{}^+ + n(OH)^- \rightarrow RuO_2 \cdot nH_2O \downarrow + NH_4OH + H^+ \quad (3)$$

Fig. 1 shows the, variation of the weight of RuO_2 thin film deposited on the substrates with the deposition time. The highest amount of RuO_2 was deposited on the glass and SS substrates were 0.320 and 0.529 mg cm^{-2}, respectively. Different growth kinetics of RuO_2 was observed on to the different kinds of substrates. Inset of Fig. 1 shows photographs of the RuO_2 deposited on the glass and SS substrates.

3.2. Structural characterization

Film crystallinity was analyzed using X-ray diffraction. The XRD patterns of RuO_2 films onto the glass and stainless steel substrates

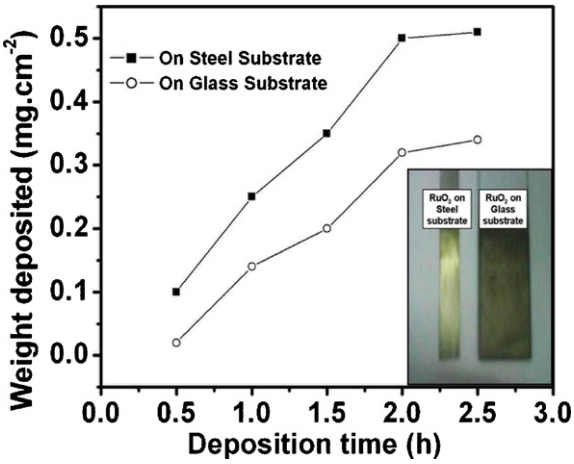

Fig. 1. Variation of weight deposited of RuO_2 with deposition time on glass and stainless steel substrates and inset shows the photograph of the RuO_2 thin film.

are shown in Fig. 2. The XRD patterns of RuO_2 thin films consist of broad hump (Fig. 2a) and no well-defined diffraction peaks other than stainless steel (Fig. 2b), indicating that amorphous nature of RuO_2 film. The obtained amorphous phase is feasible for supercapacitor application, since the protons can easily permeate through the bulk of the amorphous RuO_2 electrode and whole amount of electrode is utilized [21].

3.3. FT-IR study

The FT-IR absorption spectrum of RuO_2 in the range 4000–400 cm^{-1} is shown in Fig. 3. The strong band (ν_1) around at 600 cm^{-1} is associated with the characteristic vibrational mode of rutile RuO_2 [22]. The absorption peak (ν_2) at around 1095 cm^{-1} is assigned to characteristic stretching vibration of peroxo groups [23]. The absorption peak around at 1604 cm^{-1} is due to the bending vibration of hydroxyl groups of molecular water (ν_3) [24]. The sharp absorption band (ν_4) at 3406 cm^{-1} is attributed to the stretching vibrations of OH^- [25]. Shoulder of the ν_4 bond attributed to the hydrous nature of the RuO_2 material. These results revealed that, deposited film contained hydroxide bonds indicates the formation of hydrous RuO_2.

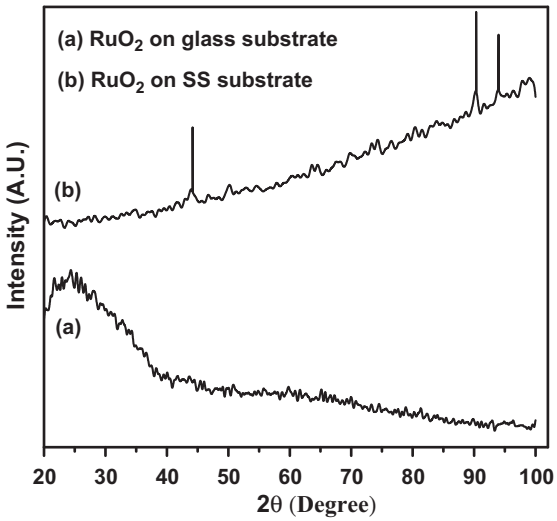

Fig. 2. X-ray diffractograms of RuO_2 thin film on (a) glass and (b) stainless steel substrates.

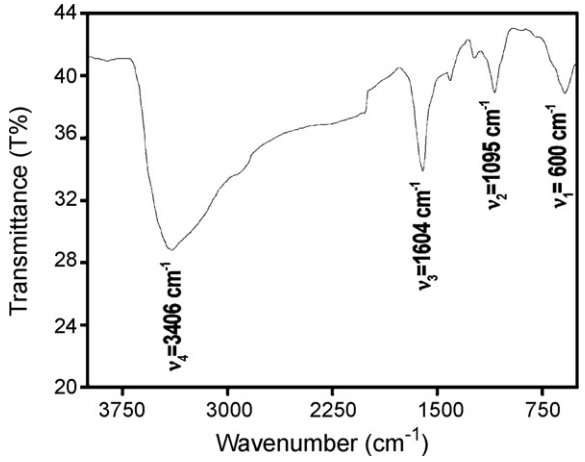

Fig. 3. FT-IR spectra of RuO_2 deposited by CBD method.

3.4. Surface morphology

Fig. 4 shows the SEM images of RuO_2 thin films. At 2000× magnification, a spherical grained particle of RuO_2 were clearly seen (Fig. 4a), whereas, at higher magnification (50,000×, Fig. 4b) a porous microstructure of RuO_2 is observed. The RuO_2 thin film had porous microstructures with fractal-like agglomerates of fine particles. Whereas, Patake and Lokhande has been reported the compact structure of RuO_2 synthesized by M-CBD method [26]. Such porous morphology may lead to the high specific surface area and porous volume, which provides the structural foundation for electrochemical processes [27].

The contact angle is expected to depend upon local inhomogeneity, chemical composition and the surface morphology of thin film. In the present case, the water laid flat with contact angle of 10° on the surface of RuO_2 film in sheets instead of forming droplet as seen in inset of Fig. 4b. This specific property is attributed to hydrous and porous nature of the material causes the superhydrophilic nature of RuO_2 [28].

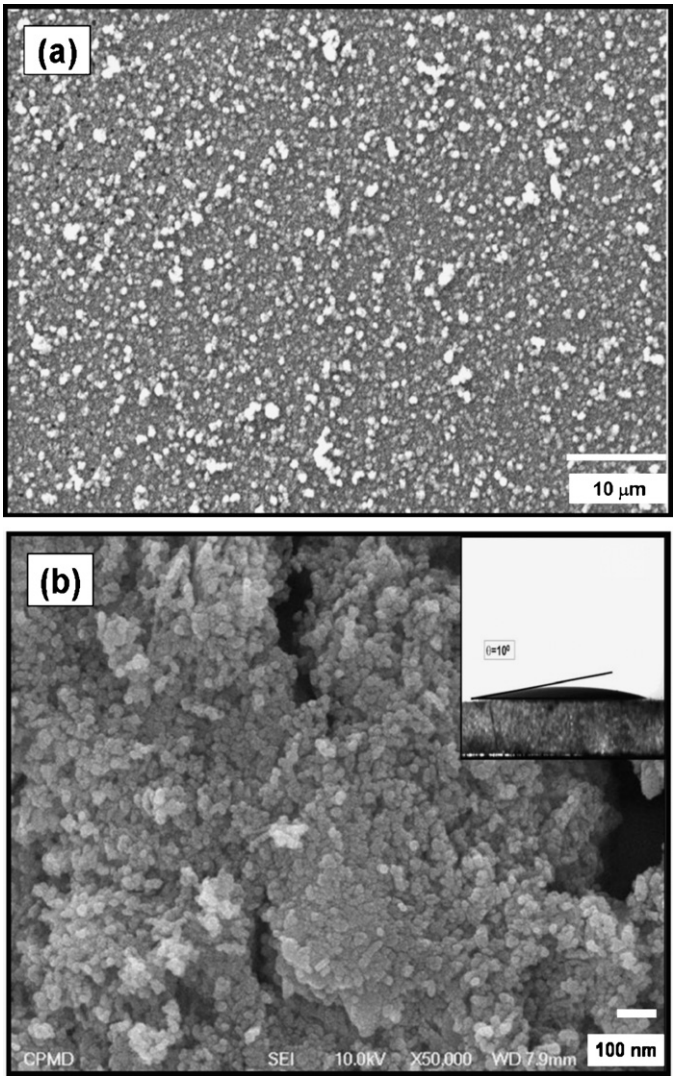

Fig. 4. SEM micrographs of RuO_2 thin films at (a) (2000×) and (b) (50,000×) magnifications. Inset of (b) shows water contact angle of RuO_2 thin films.

3.5. Optical absorption study

The optical absorption spectrum of RuO_2 film deposited onto glass substrate was studied in 350–650 nm wavelength range. The nature of the transition involved (direct or indirect) during the absorption process was determined by studying the dependence of absorption coefficient, (α) on photon energy ($h\nu$). The absorption spectrum of RuO_2 thin film is shown in inset of Fig. 5. The spectrum revealed that RuO_2 film has high absorbance coefficient (10^5 cm^{-1}), which indicates the direct transition in RuO_2 thin films. The optical data was further analyzed to determine the nature of transition that takes place in RuO_2 thin film. The plot of $(\alpha h\nu)^2$ vs. ($h\nu$) showed a straight line also indicating a direct band gap depicted in Fig. 5. The straight-line portion is extrapolated to the energy axis to obtain the band gap of the RuO_2 thin film. The direct optical band gap of RuO_2 thin film was estimated to be 2.7 eV. Patake et al. and Gujar et al., reported optical band gap of RuO_2 was 2.2 and 2.4 eV prepared by M-CBD and spray pyrolysis methods, respectively [26,29].

3.6. Electrical resistivity

Fig. 6 shows the variation of log(ρ) with reciprocal of temperature for the RuO_2 thin film on glass substrate. The resistivity at room temperature (300 K) was found to be 10^3 Ω cm. This result is analogous with the M-CBD deposited RuO_2 film reported by Patake and Lokhande [26]. The RuO_2 film resistivity decreased with increase in temperature indicating a semiconducting electrical behavior, while the metallic behavior was observed for metal organic chemically deposited (MOCVD) RuO_2 film [30]. Two trends of resistivity were observed in low (<420 K, regime I) and high (>420 K, regime II)

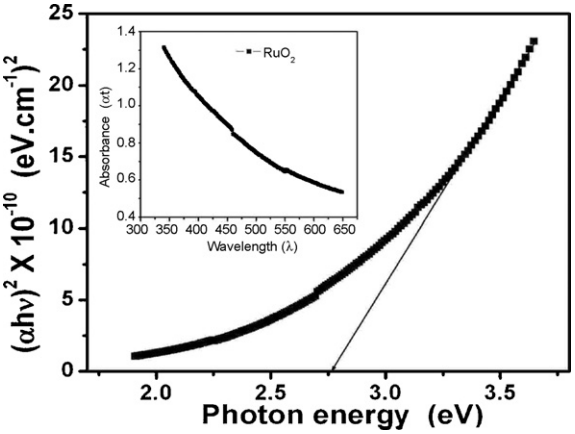

Fig. 5. Plot of $(\alpha h\nu)^2$ vs. energy ($h\nu$) of RuO_2 film. Inset shows variation of absorption (αt) with wavelength (λ) of RuO_2 film.

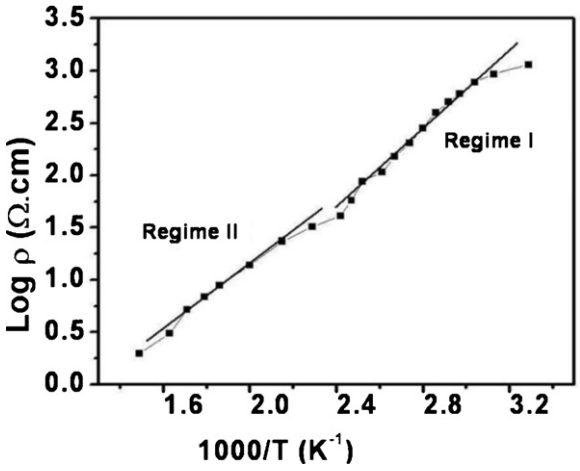

Fig. 6. The variation of electrical resistivity ($\log \rho$) with reciprocal of temperature ($1000/T$) of RuO_2 films.

temperature regions. The corresponding activation energies at low and high temperature regions were found to be 0.11 and 0.98 eV, respectively. Such change in the graphical trend after temperature regime I ascribed the removal of hydroxyl species.

3.7. Supercapacitive behavior of hydrous RuO_2 thin film

The CBD deposited hydrous RuO_2 electrodes were used in the supercapacitor and their performance were tested using cyclic voltametry (CV). The supercapacitor studies carried out by forming an electrochemical cell as hydrous RuO_2 is a working electrode, platinum as a counter electrode with SCE as a reference electrode in 0.5 M H_2SO_4 electrolyte. The supercapacitive study was carried out by means of effect of scan rate on specific/interfacial capacitance. The specific capacitance ($F\,g^{-1}$) of the electrode was obtained by dividing the capacitance to weight dipped in the electrolyte. The interfacial capacitance ($F\,cm^{-2}$) was obtained by dividing the capacitance to area dipped in the electrolyte.

Typical cyclic voltammetric (CV) behavior of hydrous RuO_2 in 0.5 M H_2SO_4 at 20 mV s^{-1} with varying the upper potential limit is shown in Fig. 7. The electrochemical evaluation revealed the pseudocapacitive behavior of the hydrous RuO_2. A voltage dependent CV plot depicted the transition peaks of Ru^{+4} with different shapes of curves analogous with report of Conway [31]. All CV's indicate that the redox transitions of oxyruthenium species within hydrous RuO_2 are highly reversible, which meets the high-power requirement for the application of supercapacitors. The shape of the CV curve within potential limit 0 to +800 mV/SCE is rectangular-like, indicating the highly reversible redox transitions of electrode. While, a tail shaped CV curve exhibited within the potential window 0 to +1000 mV/SCE, indicates the non-reversible redox reaction. Results suggest that, the CBD deposited amorphous hydrous RuO_2 favors highly ideal capacitive behavior within potential window 0 to +800 mV/SCE. The amorphous structures of hydrous RuO_2 retaining facile transport pathways for both protons and electrons since the redox transitions occur according to the following reaction.

$$RuO_x(OH)_y + wH^+ + we^- \Leftrightarrow RuO_{x-w}(OH)_{y+w} \quad (0 \le w \le 2) \qquad (4)$$

The CV response of hydrous RuO_2 electrode at different scan rates from 2 to 100 mV s^{-1} within potential window 0 to +800 mV/SCE is shown in Fig. 8a. Fig. 8a showed that voltammetric currents are directly proportional to the scan rate of CV, indicating an ideally capacitive behavior [32]. Variation of specific capacitance and interfacial capacitance values with scan rate is shown in Fig. 8b. The specific and interfacial capacitance values are decreased from 73 to 21 $F\,g^{-1}$ and 1.8 to 0.58 $mF\,cm^{-2}$, respectively, as the scan rate increases. The decrease in capacitance is attributed to the presence of inner active sites that cannot sustain the redox transitions completely at higher scan rates. This is probably due to the diffusion effect of protons within the electrode. The decreasing capacitance suggests that, parts of the surface of the electrode are inaccessible at high charging–discharging rates. Hence, the specific capacitance obtained at the slowest scan rate is believed to be closest to that of

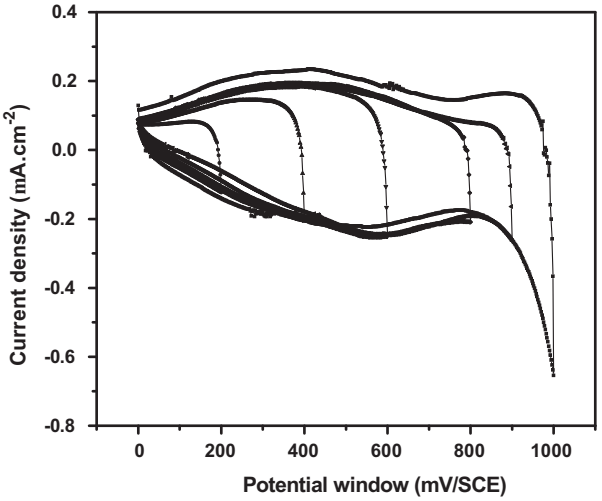

Fig. 7. CV curves of hydrous RuO_2 on SS substrate with varying the upper potential limit in 0.5 M H_2SO_4 electrolyte at 20 mV s^{-1}.

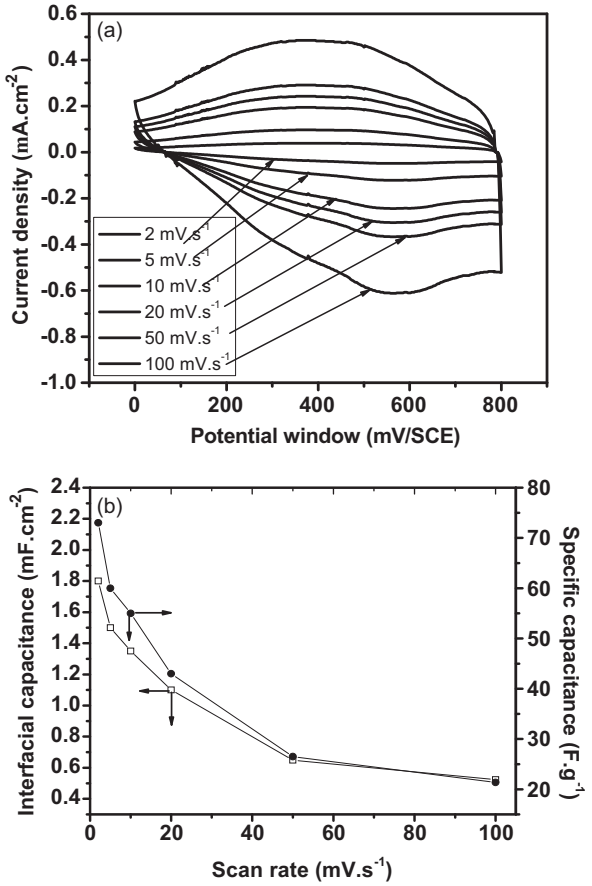

Fig. 8. (a) CV curves of hydrous RuO_2 electrode at different scanning rates. (b) Variation of interfacial and specific capacitances with scan rate.

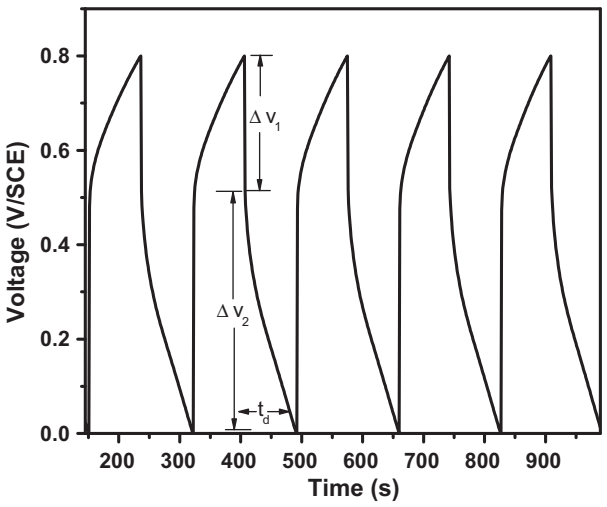

Fig. 9. Galvanostatic charge–discharge curve recorded at 100 μA cm^{-2} for the hydrous RuO_2 thin film.

full utilization of the electrode material [12]. However, Patake and Lokhande reported maximum specific capacitance 50 F g^{-1} of RuO_2 synthesized by M-CBD method on Ti substrate [26].

Charge/discharge galvanostatic plot measured at 100 μA cm^{-2} is shown in Fig. 9. The observed non-linearity in charge–discharge profile, which deviate from the typical linear variation of voltage with time, normally exhibited by a EDLCs, can be explained as due to the pseudocapacitance arising out of the redox reaction at this voltage range. At the beginning of the charge and the discharge, a sharp change in voltage (ΔV_1) due to the equivalent series resistance (ESR) of the electrochemical capacitor cell. The electrical parameters such as, specific power (SP), specific energy (SE) and coulombic efficiency (η%) are found to be 0.151 kW kg^{-1}, 3.57 Wh kg^{-1} and 94%, respectively. The values of SP, SE lies in the ragon plot typically calculated for supercapacitor [33].

The Electrochemical Impedance Studies (EIS) (in frequency 10^5–10^{-2} Hz) of hydrous RuO_2 is carried out in 0.5 M H_2SO_4. The complex-plane plot shown in Fig. 10a, consists of a small semicircle at higher frequencies with a transition to a linear part at low frequencies which corresponds to a capacitive behavior. An impedance arc of a semicircle is visible in the high frequency region (≥100 Hz) (shown in inset of Fig. 10a), attributed to the complicated interfaces at the RuO_2–RuO_2 particles and RuO_2–substrate contacts since electron hopping at these interfaces occurs during the charge/discharge processes. At low-frequencies, an approximately vertical increase in Z'' is appeared, demonstrates typical capacitive characteristics, which should be governed by the faradaic reactions of hydrous RuO_2 between different oxidation states. Similar impedance spectra is also reported for sol–gel prepared $RuOx{\cdot}nH_2O$ and MnO_2 [34,35], which have been attributed to their mesoporous and 3D network nanostructures. The ESR of the hydrous RuO_2 film arises from contact resistance of substrate is found to be 2.6 Ω [14]. Fig. 10b shows a plot of phase angle and real capacitance (C') vs. frequency; at a phase angle of 39° and 73° about 78% and 29% of the power correspond to heat production at the internal resistance with a loss factor of electrode 1.23 and 0.30 is calculated in the higher and lower frequency region, respectively. This is also in good agreement with the effect of scan rate on specific capacitance, wherein specific capacitance is higher for lower scan rate and it decreases for higher value. Therefore lower scan rate is appropriate for good performance of hydrous RuO_2 electrode. The relaxation time constant (τ_0) is calculated from plots of C' (ω) vs. frequency and it is found to 0.63 s. The τ_0 is very important factor, which decides the applicability of electrode material according to energy demand. Smaller

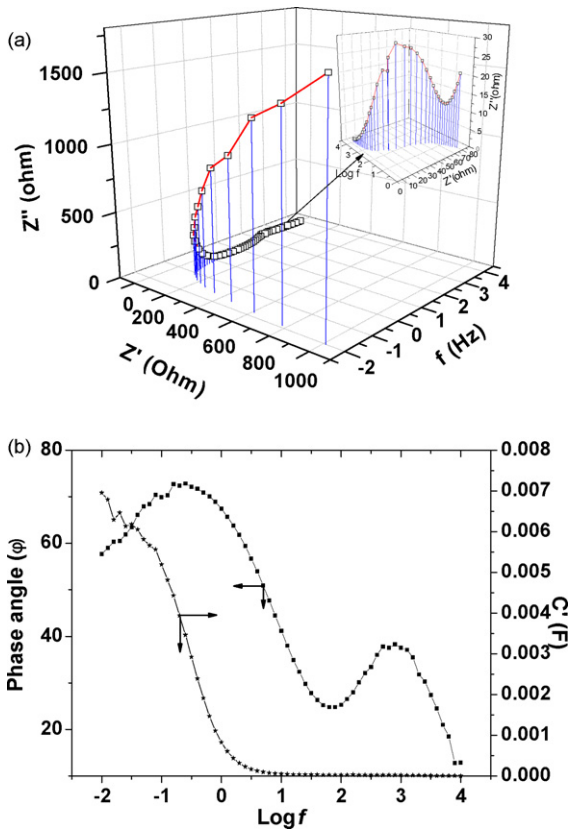

Fig. 10. (a) Complex-plane plot and (b) plot of phase angle (ϕ) and real capacitance (C') vs. frequency (log f) of hydrous RuO_2 electrode in 0.5 M H_2SO_4.

relaxation time constant value exhibits a faster energy release capability of electrode, so that provide higher power density [36]. A new synthesis technique based on CBD is introduced which yields to deposit hydrous RuO_2 with specific capacitance 73 F g^{-1} on stainless steel substrate. The strong influence of ESR, power corresponds to heat production due to internal resistance of hydrous RuO_2 thin film may limit to achieve the maximum reported specific capacitance [12–16]. The specific capacitance of hydrous RuO_2 can be enhanced by lowering ESR by reducing contact resistance, using the different kinds of substrates like (Ti, Au, etc.).

4. Conclusions

In conclusion, the amorphous hydrous RuO_2 thin films (confirmed from XRD and FT-IR studies) have been successfully synthesized at low temperature on glass and SS substrates using lucrative CBD method which is single step, simple, easy, and efficient. SEM images reveal that porous and spherical grained morphology of films. The optical and electrical study showed a direct band gap of hydrous RuO_2 thin films to be 2.7 eV with semiconducting nature. The ESR, power corresponds to heat production due to internal resistance and higher loss factor of hydrous RuO_2 thin film restricts maximum specific capacitance up to the 73 F g^{-1}. The specific power (SP), specific energy (SE) and coulombic efficiency (η%) of electrode is found to be 0.151 kW kg^{-1}, 3.57 Wh kg^{-1} and 94%, respectively. However, the electrodes having small storage capacity with less relaxation time (0.63 s), so it can be used in the devices that require small energy can deliver in very short time.

Acknowledgement

Authors are grateful to the Council of Scientific and Industrial Research (CSIR), New Delhi for financial support through the scheme no. 03(1165)/10/EMR-II.

References

[1] C.C. Hu, W.C. Chen, K.H. Chang, J. Electrochem. Soc. 151 (2004) A281.
[2] B. Cornell, D. Simonsson, J. Electrochem. Soc. 140 (1993) 3123.
[3] S. Hadzi-Jordanov, H. Angerstein-Kozlowska, M. Vukovic, B.E. Conway, J. Electrochem. Soc. 125 (1978) 1471.
[4] S. Trasatti, G. Buzzanca, J. Electroanal. Chem. 29 (1971) 1.
[5] K. Doblhofer, M. Metikos, Z. Ognmi, H. Gerischer, B. Bunsenges, Phys. Chem. 82 (1978) 1046.
[6] S. Sarangapani, B.V. Tilak, C.P. Chen, J. Electrochem. Soc. 143 (1996) 3791.
[7] S. Trasatti, in: A. Wieckowski (Ed.), Interfacial Electrochemistry Theory, Experiment and Applications, Dekker, New York, 1999, p. 769.
[8] S. Ferro, A. De Battisti, J. Phys. Chem. B 106 (2002) 2249.
[9] J.P. Zheng, T.R. Jow, J. Power Sources 62 (1996) 155.
[10] J.L. Gomez de la Fuente, M.V. Martınez-Huerta, S. Rojas, P. Hernandez-Fernandez, P. Terreros, J.L.G. Fierro, M.A. Pena, Appl. Catal. B: Environ. 88 (2009) 505.
[11] D. Galizzioli, F. Tantardini, S. Trasatti, J. Appl. Electrochem. 4 (1974) 57.
[12] D.A. McKeown, P.L. Hagans, L.P.L. Carette, A.E. Russell, K.E. Swider, D.R. Rolison, J. Phys. Chem. B 103 (1999) 4825.
[13] W. Dmowski, T. Egami, K.E. Swider-Lyons, C.T. Love, D.R. Rolison, J. Phys. Chem. B 106 (2002) 12677.
[14] J.P. Zheng, P.J. Cygan, T.R. Jow, J. Electrochem. Soc. 142 (1995) 2699.
[15] H. Kim, K.B. Kim, J. Electrochem. Soc. 153 (2006) A383.
[16] B.O. Park, C.D. Lokhande, H.S. Park, K.D. Jung, O.S. Joo, J. Power Sources 134 (2004) 148.
[17] F. Pico, J. Ibanez, M.A. Lillo-Rodenas, A. Linares-Solano, R.M. Rojas, J.M. Amarilla, J.M. Rojo, J. Power Sources 176 (2008) 417.
[18] C.C. Hu, K.H. Chang, C.C. Wang, Electrochim. Acta 52 (2007) 4411.
[19] R.S. Mane, C.D. Lokhande, Mater. Chem. Phys. 65 (2000) 1.
[20] C.D. Lokhande, Mater. Chem. Phys. 27 (1991) 1.
[21] D.R. Rolison, P.L. Hagans, K.E. Swider, J.W. Long, Langmuir 15 (1999) 774.
[22] J. Mink, J. Kristof, A. De Battisti, S. Daolio, C. Nemeth, Surf. Sci. 335 (1995) 252.
[23] Y. Wang, N. Herron, J. Phys. Chem. 95 (1991) 525.
[24] S. Karuppuchamy, J.M. Jeong, J. Oleo Sci. 55 (2006) 263.
[25] W. Sugimoto, H. Iwata, Y. Murakami, Y. Takasu, J. Electrochem. Soc. 151 (2004) A1181.
[26] V.D. Patake, C.D. Lokhande, Appl. Surf. Sci. 254 (2008) 2820.
[27] U.M. Patil, K.V. Gurav, V.J. Fulari, C.D. Lokhande, O.S. Joo, J. Power Sources 188 (2009) 338.
[28] A.V. Rao, S.S. Latthe, D.Y. Nadargi, H. Hirashima, V. Ganesan, J. Colloid Interface Sci. 332 (2009) 484.
[29] T.P. Gujar, V.R. Shinde, C.D. Lokhande, W.Y. Kim, K.D. Jung, O.S. Joo, Electrochem. Commun. 9 (2007) 504.
[30] P.K. Baumann, P. Doppeil, K. Frohlich, L. Gueroudji, V. Cambel, O. Machajdik, M. Schumacher, J. Lindner, F. Schlenle, D. Birgess, G. Strauch, H. Juergensen, H. Guillon, C. Jimenez, Integr. Ferroelectr. 44 (2002) 135.
[31] B.E. Conwey, Electrochemical Supercapacitors: Scientific Fundamentals and Technological Applications, Kluwer Academic/Plenum Publishing, New York, 1999.
[32] J.N. Broughton, M.J. Brett, Electrochem. Solid State Lett. 5 (2002) A279.
[33] A. Bruke, J. Power Sources 91 (2000) 37.
[34] C.C. Hu, W.C. Chen, Electrochim. Acta 49 (2004) 3469.
[35] C.C. Hu, C.C. Wang, J. Electrochem. Soc. 150 (2003) 1079.
[36] V. Ganesh, S. Pitachumani, V. Lakshminarayanan, J. Power Sources 158 (2006) 1523.